








## Tuneable plasmonic gold dendrimer nanochains for sensitive disease detection†

Antonio J. Ruiz-Sanchez, \* Claudio Parolo,  Benjamin S. Miller,   
Eleanor R. Gray,  Kristina Schlegel and Rachel A. McKendry \*

Cite this: *J. Mater. Chem. B*, 2017, 5, 7262

Received 22nd May 2017,  
Accepted 1st August 2017

DOI: 10.1039/c7tb01394a

rsc.li/materials-b

**We report the development of a tuneable plasmonic nanochain immunoassay with increased sensitivity over traditional mono-disperse nanoparticle lateral flow tests. Our approach takes advantage of the unique self-assembling properties of polyamidoamine dendrimers with gold nanoparticles in aqueous media to create one-dimensional nanochains, with a distinct red to blue colour change, attributable to a longitudinal plasmon resonance, which can be readily detected by eye and a digital camera. We optimise and characterise nanochain formation and stability using UV-visible spectroscopy, transmission electron microscopy and dynamic light scattering. As a proof-of-principle we focus on the application of nanochains for point-of-care diagnostics for p24, an important biomarker of early HIV infections and successfully detect p24 with a limit of detection of 5 ng ml<sup>-1</sup> in pseudo-serum, 4 fold more sensitive than comparable studies with gold nanoparticles. These findings and underlying concepts highlight the potential of advanced functional organic–inorganic composite nanomaterials to diagnose infections, with broad applicability to non-communicable diseases.**

Infectious diseases rank among the gravest threats to human health. HIV, Ebola, Zika virus underline the urgent need for new diagnostics tests for use at the point-of-care (PoC).<sup>1</sup> A late HIV diagnosis has serious consequences for the individual because treatment is delayed – leading to increased suffering and reduced life expectancy. Late diagnosis also has consequences for society due to the increased risk of onwards transmission by people who are unaware of their infection.<sup>2</sup> Gold standard diagnostic tests, such as enzyme linked immunosorbent assays (ELISA), are well embedded in tertiary laboratories around the globe, but they typically require samples to be sent by cold-chain transportation, leading to significant turn-around times, and also require large and expensive equipment and trained personnel.<sup>3</sup> These characteristics limit their use in PoC settings. The ASSURED

requirements for PoC tests state that they should be: Affordable, Specific, Sensitive, User-friendly, Rapid and Robust, Equipment-free and Delivered to those in need. ASSURED diagnostics could revolutionise PoC testing, and support faster initiation of care and treatment, leading to improved health and economic outcomes.<sup>4</sup>

Lateral flow immunoassays (LFIAs) fulfil many of the ASSURED criteria and are widely used for diagnosis of infectious diseases (e.g. HIV, flu) and other outcomes (e.g. pregnancy). The fundamental principle is simple and relies on the natural capillary-driven flow of a sample along a nitrocellulose paper microfluidic strip. The presence of a biomarker of infection is typically detected by a sandwich immunoassay between a Test line of capture ligands, a biomarker in solution, and gold nanoparticles (AuNP) tailored with a complementary capture ligand in solution. A positive result typically gives rise to a visible red coloured test line within 5–20 minutes. The manufacturing cost per LFIA test is typically less than 1 US dollar.<sup>5</sup> Nevertheless, LFIAs have limitations that impede their use in a wider range of diagnostic applications, primarily a lack of sensitivity means that it is difficult to detect very low concentrations of target protein, leading to the risk of false negative results and missed opportunities to access potentially life-saving treatment. Moreover, LFIAs are notoriously difficult to interpret. Indeed, a recent behaviour study of HIV self-tests showed that only 26% of naïve testers, who had not been trained to use the tests, correctly interpreted a weak positive result.<sup>6</sup>

Herein we report the development of a novel plasmonic nanomaterials-based approach to overcome the limitations of LFIA sensitivity, potentially making these tests easier to interpret and more user friendly. Our novel approach harnesses the self-assembly of AuNPs with well-defined monodisperse polyamidoamine (PAMAM) dendrimers to build one-dimensional nanochain-like structures. These nanochains have two key advantages over traditional mono-dispersed AuNPs. Firstly, the characteristic plasmonic bands confer a strong blue colour, which is easily detectable by eye as a positive result and distinct from a red control line used in lateral flow tests. Secondly, the presence of

London Centre for Nanotechnology and Division of Medicine,  
University College London (UCL), 17-19 Gordon Street, London WC1H 0AH, UK.

E-mail: [ajruizs@gmail.com](mailto:ajruizs@gmail.com), [r.a.mckendry@ucl.ac.uk](mailto:r.a.mckendry@ucl.ac.uk)

† Electronic supplementary information (ESI) available. See DOI: 10.1039/c7tb01394a



a chain of multiple nanoparticles in principle increases the sensitivity compared to a single nanoparticle label. PAMAM dendrimers are monodispersed, highly branched, globular polymers.<sup>7</sup> The multimeric cationic properties of their primary amine end groups have been used in a range of biomedical applications, for example in the formation of DNA/PAMAM complexes in non-viral gene delivery<sup>8</sup> and drug delivery.<sup>9</sup> A number of experimental and theoretical studies have explored the self-assembly of dendrimer-gold nanoparticle composites but typically they form random, amorphous aggregates driven by electrostatic interactions between positively charged dendrimers and negatively charged AuNPs. Such aggregates are far from ideal for LFIA and can lead to poor reproducibility, and potentially clog tests. Although some researchers have shown that AuNPs can form organised into one dimensional structures, this is typically non-trivial, and requires a special template<sup>10</sup> or organic solvents which can denature protein coatings.<sup>11,12</sup> By contrast, we demonstrate that stable gold-dendrimer nanochains can be readily formed in aqueous media, without the need for templates or organic solvents by tuning the density of dendrimers physisorbed onto each nanoparticle (Fig. 1). We also demonstrate that this organic-inorganic hybrid plasmonic nanomaterial significantly improves the performance characteristics of LFIAs using model recombinant protein samples.

The preparation of gold-dendrimer-nanochains (GDnC-X) is shown schematically in Fig. 2, where the suffix-X represents the number of molar equivalents of PAMAM dendrimer compared to AuNP. Details of the full synthesis are given in (ESI†) but in brief, different GDnC-X were obtained by the addition of 30  $\mu$ l of PAMAM G5 dendrimer aqueous solution at different concentrations (0–200 nM) to 300  $\mu$ l of commercial citrate-capped AuNP (1.2 nM), the most common label in commercial LFIAs.<sup>5</sup> PAMAM G5 dendrimers were selected due to their highly dense cationic surface charge (128 primary amines) that can interact with the anionic AuNPs. Immediately after the addition of the dendrimers, the colour of the suspension changed and could be tuned from a deep red to purple or blue by varying the molar ratio  $X$  (Fig. 3).

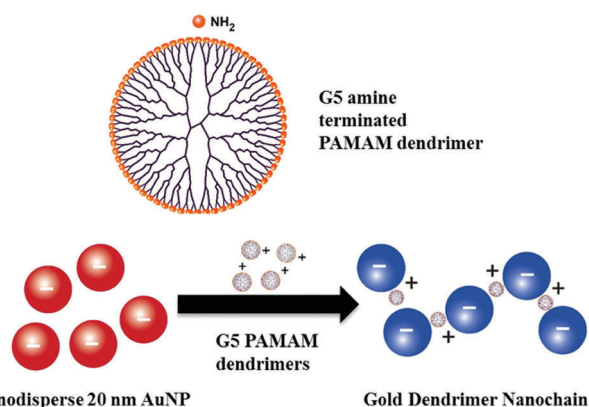


Fig. 1 Schematic to show the chemical structure of a Generation 5 PAMAM dendrimer and the proposed self-assembly mechanism of dendrimers with 20 nm gold nanoparticles to generate one dimensional 'nanochains', driven by electrostatic interactions.

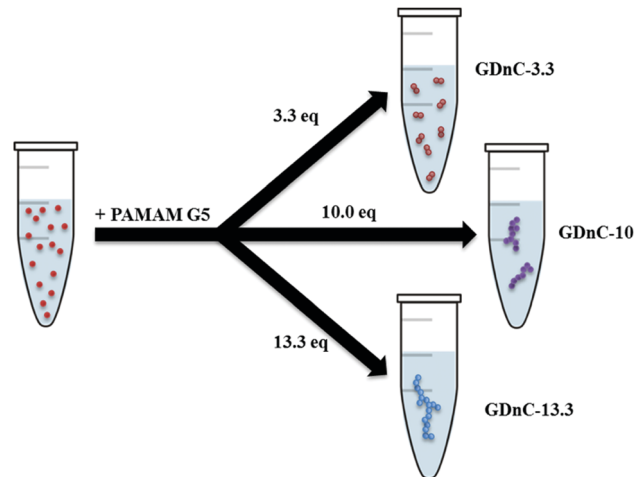


Fig. 2 Schematic to illustrate the synthesis of gold-dendrimer-nanochains (GDnC-X) by tuning the number of molar equivalents of PAMAM dendrimer (denoted by suffix X) added in relation to of AuNP.

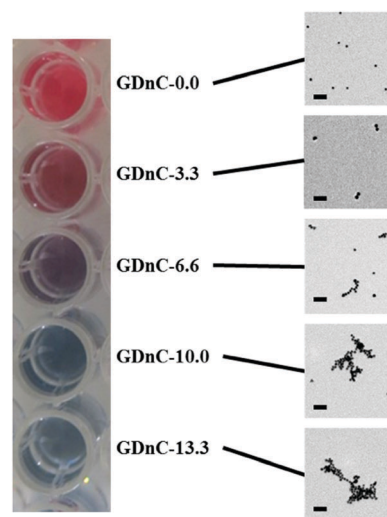


Fig. 3 A digital photographic image of the resulting colour of different gold-dendrimer nanochains GDnC-X prepared in a 96 well plate on the left, and the respective characterisation of each GDnC-X by transmission electron microscopy (TEM). The scale bar on the TEM images represents 100 nm.

We characterised the plasmonic properties, stability, physical morphology and electrophoretic properties of GDnC-X nanocomposites using a range of methods, including UV-Vis Spectroscopy, Dynamic Light Scattering (DLS), Electrophoretic Light Scattering (ELS) and Transmission Electron Microscopy (TEM). Fig. 4A shows the UV-Vis spectra of freshly prepared samples of GDnC-Xs compared to AuNPs with no dendrimers (GDnC-0.0) (red line). Increasing  $X$  (the number of molar equivalents of PAMAM dendrimer compared to AuNP) led to a notable decrease in the intensity of the first plasmonic resonance peak at 524 nm and the appearance of a new second peak between 600 and 800 nm. The appearance of the second peak indicates that these aggregates are not randomly formed, but have a preferred spatial distribution.<sup>13</sup> This is the first time such a band has been seen



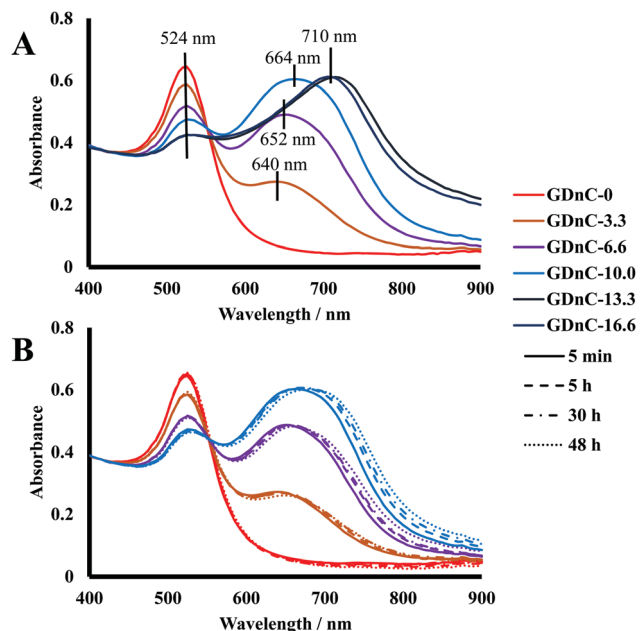


Fig. 4 (A) UV-visible spectra of different GDnC-*X* shows a distinct red to blue shift with increasing dendrimer equivalents (*X*), compared to a reference solution of gold-nanoparticles with no dendrimers (red line); (B) UV-vis spectra for GDnC-0, GDnC-3.3, GDnC-6.6 and GDnC-10.0 after 5 min, 5 h, 30 h and 48 h of preparation.

for dendrimer-gold nanochains and this longitudinal plasmon band<sup>14</sup> is characteristic of gold nanorods, nanochains and nanowires and is due to the excitation of plasmon resonance along their long axis. We observed that the longitudinal plasmon band of the GDnC ( $\lambda$ -LPR) increases in intensity and shifts to higher wavelength, from 640 nm to 710 nm for  $X = 3.3$ –13.3 respectively, as the number of equivalents of PAMAM increases, suggesting a direct influence of dendrimer concentration on the formation of GDnCs. For dendrimer additions up to 10 equivalents, an isosbestic point at 552 nm is observed, indicating that the species involved are linearly related by stoichiometry. For higher values of dendrimers, the isosbestic point is lost, thus the linear relation within these aggregates has disappeared.

UV-visible spectroscopy was also used to investigate the stability of our nanocomposites over periods of 5 min, 5 hours, 30 hours and 48 hours. The spectra of GDnC-3.3, GDnC-6.6 and GDnC-10 did not change noticeably, demonstrating good stability (Fig. 4B). The samples of GDnC-13.3 and GDnC-16.6 formed precipitates within a few minutes, showing that these structures are unstable in solution.

While UV-vis analysis is sensitive to the aggregation of materials in suspension,<sup>15</sup> it is unable to accurately discern the physical size or geometry of the nanochains, and therefore we turned to DLS and TEM. Table 1 shows that the average mean hydrodynamic diameter measured by DLS increases with  $X$  from  $29.4 \pm 4$  nm, to  $49.4 \pm 3.5$ ,  $90.5 \pm 2.4$ ,  $98.5 \pm 1.4$ ,  $124.8 \pm 1.2$  and  $505.2 \pm 51.2$  for  $X = 0$ , 3.3, 6.6, 10.0, 13.3 and 16.6 respectively. The respective morphologies can be observed in the TEM images in Fig. 3. Although the dendrimers cannot be seen in these images, there is a striking change in morphology

**Table 1** Table to show the characterisation of different GDnC-*X* complex using Dynamic Light Scattering (DLS), including the mean diameters as determined from the intensity (nm), L-SPR peak position (nm), polydispersity index (PI) and  $\zeta$ -potential. Average mean and standard deviation obtained from three independent experiments. For  $\zeta$ -potential, measurements were only made to the chosen GDnC-*X*

GDnC- <i>X</i> , where <i>X</i> =	DLS diameter (nm)	PI	$\lambda$ -LPR (nm)	$\zeta$ potential (mV)
0	$29.4 \pm 0.4$	0.16	—	$-42.4 \pm 2.4$
3.3	$49.4 \pm 3.5$	0.38	640	—
6.6	$90.5 \pm 2.4$	0.44	652	$-27.9 \pm 1.3$
10.0	$98.5 \pm 1.4$	0.28	664	—
13.3	$124.8 \pm 1.2$	0.253	710	$-19.8 \pm 2.3$
16.6	$505.2 \pm 51.2$	0.666	710	—
6.6-Ab	$88.6 \pm 3.3$	0.359	652	—
825	$29.7 \pm 1.1$	0.183	—	$+7.8 \pm 0.2$

with increasing dendrimer concentrations – initially we see a uniform distribution of individual nanoparticles for  $X = 0$ , then pairs of nanoparticles (dimers) are observed for  $X = 3.3$ , followed by elongated chain-like structures for  $X = 6.6$  and nets of chains and random aggregates for  $X = 10.0$  and 13.3. We note that a close inspection of the TEM images shows that not all nanoparticles assemble into dimers or nanochains and isolated individual AuNPs are also observed for GDnC-3.3, GDnC-6.6 and GDnC-10.0 but not in GDnC-13.3.

Next, we characterised their electrophoretic mobility using ELS in order to obtain  $\zeta$ -potential values (as reported in Table 1) for GDnC-0, GDnC-6.6 and GDnC-13.3. All measurements were repeated in triplicate. As expected, the addition of positively charged PAMAM dendrimers to negatively charged AuNP, shifted the initial  $\zeta$ -potential of  $-42.4 \pm 2.4$  mV ( $X = 0$ ) to increasingly more positive values of  $-27.9 \pm 1.3$  ( $X = 6.6$ ) and  $-19.8 \pm 2.3$  mV ( $X = 13.3$ ). These findings strongly support the hypothesis that nanochain formation is driven by electrostatic interactions. To further test the role of electrostatic interactions, we investigated the effect of high pH and high salt concentrations, which should in principle minimise electrostatic forces by deprotonating dendrimer amine groups and reducing the Debye length. As expected an increase in pH of a suspension of AuNP *via* addition of NaOH, led to no aggregation. Intriguingly, however, we observed that an excess of added sodium citrate over a suspension of AuNP did not prevent the formation of GDnC-*X*. This suggests that more experimental and theoretical modelling work is needed to understand the mechanism of nanochain formation. Finally, we were interested to test the influence of very high dendrimer concentrations ( $X = 825$ ), which we anticipated would saturate all possible binding sites on the gold nanoparticles and inhibit nanochain formation. As expected we observed no aggregation and the measured  $\zeta$ -potential showed a value of  $+7.8$  mV.

Having characterised different gold-dendrimer nanochains, we next sought to select lead candidates as labels in LFIA based on their stability and size, to increase the number of antibodies available per label, maximizing the probability of analyte recognition and the sensitivity of the PoC test. On this basis, we selected GDnC-6.6 and GDnC-10.0 as our lead candidates



(GDnC-13.3 and GDnC-16.6 were not stable enough and the size of  $X = 3.3$  dimers is not significantly larger than monodispersed AuNPs).

We then functionalized GDnC-6.6 and GDnC-10.0 with a mouse monoclonal capture antibody specific to the HIV-1 antigen p24 and for comparison we functionalised monodisperse 20 nm AuNPs in an identical way to benchmark our results. We focused on the detection of p24 because it is an important biomarker of early HIV infections prior to seroconversion, when the virus is highly transmissible, because there is an unmet need for ASSURED PoC tests and thus an ideal test for our plasmonic nanochain LFIA.<sup>16</sup> The functionalization procedure is explained in details in the ESI,<sup>†</sup> but briefly colloidal suspensions were incubated with an excess of capture antibodies, followed by a blocking step with bovine serum albumin BSA protein to reduce non-specific interactions.<sup>17</sup> The excess of antibodies was removed by centrifugation, and the pellet (composed of functionalised AuNP or GDnC) was re-suspended in phosphate buffered saline. We found that it was not possible to effectively re-suspend the GDnC-10.0 nanocomposite possibly due to instability during centrifugation conditions, with resultant aggregation and precipitation. On the other hand, the functionalization of GDnC-6.6 with antibodies was very robust and the hydrodynamic diameter and  $\lambda$ -LPR were consistent with the values obtained for the functionalisation, and so we decided to proceed with solely GDnC-6.6.

We engineered a series of nitrocellulose paper microfluidic test strips, with a specific anti-p24 capture antibody Test line and a Control capture anti-mouse antibody to confirm that the test was functional (Fig. 5). We then premixed either functionalised GDnC-6.6 or AuNPs with different concentrations of recombinant p24 in a buffer of 2% BSA and 0.05% Tween 20.

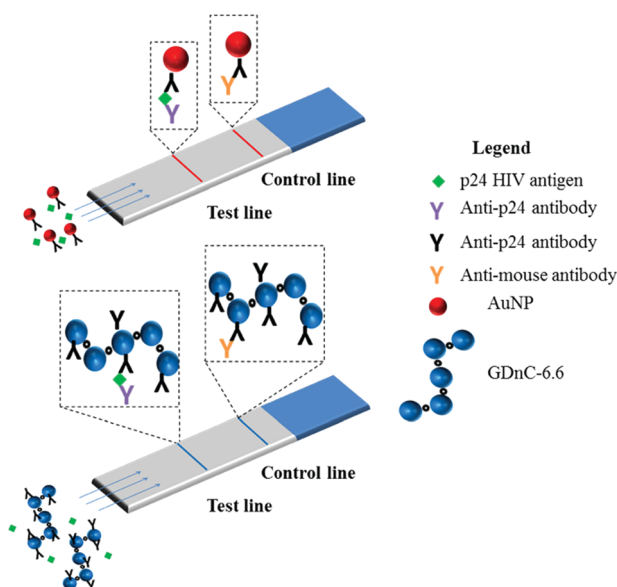


Fig. 5 A schematic to illustrate the concept of LFIA to detect HIV p24 antigen, using traditional monodisperse AuNP assays which give a distinct red test and control line; compared to gold-dendrimer nanochains (GDnC-6.6) which generate a blue coloured test and control line.

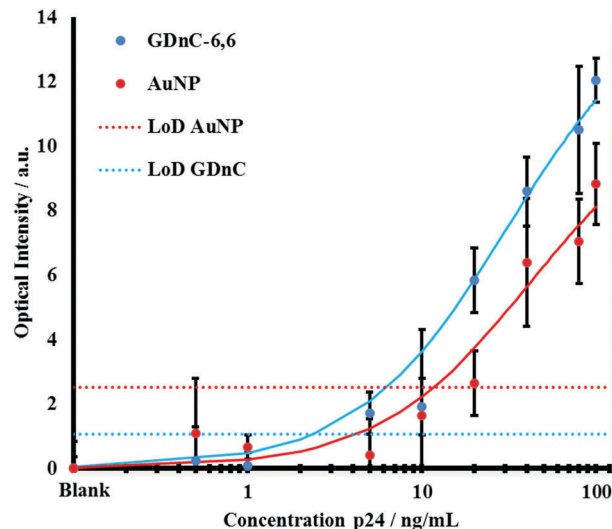


Fig. 6 A plot to compare the sensitivity of a gold-dendrimer GDnC-6.6 nanochains (blue) LFIA to detect the HIV antigen p24 compared to monodisperse gold nanoparticles AuNPs (red). The plot shows the optical intensity measured on the sandwich immunoassay on LFIA strips (Fig. 5) as a function of the concentration of recombinant p24 concentration in a model buffer solution. The solid line fit correspond to the Langmuir adsorption isotherm models ( $R^2 = 0.93$  and  $0.87$  for GDnC-6.6 and AuNPs respectively). The dashed line corresponds to the Limit of Detection (LoD, three times the standard deviation of zero concentration) for AuNPs (red dotted line) versus GDnC-6.6 (blue dotted line).

Positive test results could be readily detected by eye within minutes. The intensity of the test and control spots were quantified using a Canon G15 digital camera and analysed with Image J and Mathematica software. Fig. 6 shows a plot of the optical signal intensity as function of the concentration of p24, using both AuNP (red dots) and GDnC-6.6 (blue dots), and fitted with a Langmuir adsorption isotherm model (solid line fits,  $R^2 = 0.93$  and  $0.87$  respectively). In addition, the values of the Limit of Detection (LoD, defined as the average of 3 blank samples plus three times the standard deviation of the blank samples) are represented as a red and a blue dotted line for AuNP and GDnC-6.6 respectively. At low concentration, the signal increases with increasing p24 concentration. At higher concentrations, above  $100 \text{ ng ml}^{-1}$  we anticipate that the signal saturates, presumably when all the available binding sites are occupied. The lowest detectable concentration for GDnC-6.6 was found to be  $5 \text{ ng ml}^{-1}$  and approximately four times more sensitive than for AuNPs ( $20 \text{ ng ml}^{-1}$ ) due to a smaller LoD for the GDnC. All these experiments were reproduced in triplicate.

## Conclusions

To close, in this communication we demonstrate that the controlled self-assembly of gold nanoparticles and PAMAM G5 dendrimers into stable, functional nanochains can serve as excellent labels for LFIA with low  $\text{ng ml}^{-1}$  sensitivity and is 4 fold more sensitive than traditional monodisperse 20 nm AuNPs. This platform technology highlights the promise of advanced nanomaterials and is transferable to other infections and



non-communicable diseases; also to different transduction mechanisms such as electrochemical sensors. Future work should investigate the influence of different dendrimer generations compared to other simple polyamines, and investigate the sensitivity and specificity in real clinical samples.

## Conflicts of interest

There are no conflicts of interest to declare.

## Acknowledgements

We thank the i-sense EPSRC IRC in Early Warning Sensing Systems for Infectious Diseases (Grant reference number EP/K031953/1 [www.i-sense.org.uk](http://www.i-sense.org.uk)), Royal Society Wolfson Research Merit Award (McKendry) and Biochemical Engineering Doctoral Training Award for funding. We thank Dr Catriona M. McGilvery (Department of Materials, Imperial College London) for the TEM measurements.

## Notes and references

- J. C. Saiz, Á. Vázquez-Calvo, A. B. Blázquez, T. Merino-Ramos, E. Escribano-Romero and M. A. Martín-Acebes, *Front. Microbiol.*, 2016, 7, 1–19.
- R. O. Valdiserri, D. R. Holtgrave and G. R. West, *AIDS*, 1999, 13, 2317.
- B. M. Branson, *Clin. Infect. Dis.*, 2007, 45(suppl. 4), S221.
- P. Patel, B. Bennett, T. Sullivan, M.-M. Parker, J. D. Heffelfinger and P. S. Sullivan, *J. Clin. Virol.*, 2012, 54, 42–47.
- C. Parolo and A. Merkoci, *Chem. Soc. Rev.*, 2013, 42, 450–457.
- R. B. Peck, J. M. Lim, H. Van Rooyen, W. Mukoma, L. Chepuka, P. Bansil, L. C. Knight, N. Muturi, E. Chirwa and A. M. Lee, *et al.*, *AIDS Behav.*, 2014, 18, 422–432.
- D. A. Tomalia, H. Baker, J. Dewald, M. Hall, G. Kallos, S. Martin, J. Roeck, J. Ryder and P. Smith, *Polym. J.*, 1985, 17, 117–132.
- G. A. Brazeau, S. Attia, S. Poxon and J. A. Hughes, *Pharm. Res.*, 1998, 15, 680–684.
- S. Hong, A. U. Bielinska, A. Mecke, B. Keszler, J. L. Beals, X. Shi, L. Balogh, B. G. Orr, J. R. Baker and M. M. Banaszak Holl, *Bioconjugate Chem.*, 2004, 15, 774–782.
- H. Kitching, M. J. Shiers, A. J. Kenyon and I. P. Parkin, *J. Mater. Chem. A*, 2013, 1, 6985–6999.
- H. Zhang, K. H. Fung, J. Hartmann, C. T. Chan and D. Wang, *J. Phys. Chem. C*, 2008, 112, 16830–16839.
- J. Liao, Y. Zhang, W. Yu, L. Xu, C. Ge, J. Liu and N. Gu, *Colloids Surf., A*, 2003, 223, 177–183.
- M. Hu, J. Chen, Z.-Y. Li, L. Au, G. V. Hartland, X. Li, M. Marquez and Y. Xia, *Chem. Soc. Rev.*, 2006, 35, 1084–1094.
- I. Hussain, M. Brust, J. Barauskas and A. I. Cooper, *Langmuir*, 2009, 25, 1934–1939.
- C. S. Weisbecker, M. V. Merritt and G. M. Whitesides, *Langmuir*, 1996, 12, 3763–3772.
- P. D. Howes, S. Rana and M. M. Stevens, *Chem. Soc. Rev.*, 2014, 43, 3835–3853.
- C. Parolo, A. de la Escosura-Muñiz, E. Polo, V. Grazú, J. M. de la Fuente and A. Merkoçi, *ACS Appl. Mater. Interfaces*, 2013, 5, 10753–10759.

